

Capacity Bounds for Communication Systems with Quantization and Spectral Constraints

Sourjya Dutta, Abbas Khalili, Elza Erkip, Sundeep Rangan
Dept. of Electrical and Computer Engineering,
Tandon School of Engineering, New York University, Brooklyn, NY, USA

Abstract—Low-resolution digital-to-analog and analog-to-digital converters (DACs and ADCs) have attracted considerable attention in efforts to reduce power consumption in millimeter wave (mmWave) and massive MIMO systems. This paper presents an information-theoretic analysis with capacity bounds for classes of linear transceivers with quantization. The transmitter modulates symbols via a unitary transform followed by a DAC and the receiver employs an ADC followed by the inverse unitary transform. If the unitary transform is set to an FFT matrix, the model naturally captures filtering and spectral constraints which are essential to model in any practical transceiver. In particular, this model allows studying the impact of quantization on out-of-band emission constraints. In the limit of a large random unitary transform, it is shown that the effect of quantization can be precisely described via an additive Gaussian noise model. This model in turn leads to simple and intuitive expressions for the power spectrum of the transmitted signal and a lower bound to the capacity with quantization. Comparison with non-quantized capacity and a capacity upper bound that does not make linearity assumptions suggests that while low resolution quantization has minimal impact on the achievable rate at typical parameters in 5G systems today, satisfying out-of-band emissions are potentially much more of a challenge.

Index Terms—Quantization, millimeter wave, analog-to-digital conversion, digital-to-analog conversion, out of band emission.

I. INTRODUCTION

All digital communications systems rely on digital-analog and analog-digital converters (ADCs and DACs). In recent years, there has been considerable interest in systems with so-called *low resolution* DACs and ADCs where the number of bits is very small (typically 3-4 bits in I and Q). These architectures have attracted particular attention in the context of energy-efficient approaches for next-generation millimeter wave (mmWave) and massive MIMO systems [1]–[19]. In particular, mmWave systems rely on communication across wide bandwidths with large numbers of antennas [20], [21]. Power consumption thus becomes a key issue, particularly in so-called fully digital architectures where signals from all antennas are digitized for fast beam-tracking, initial access and spatial multiplexing [1]–[3], [7], [12].

At low resolutions, it is critical to evaluate the effect of quantization accurately, and there is now a large body of work on characterizing the capacity of such systems [8]–[10], [13]–[19], [22]. The most common model is to approximate the quantizer in either the DAC or ADC via an additive Gaussian noise (AGN) model [23], [24]. There are several works that provide rigorous analysis of the AGN model under variety of assumptions such as the high rate regime or dithered

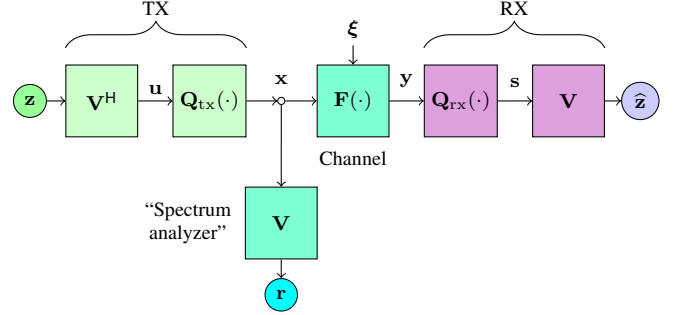


Fig. 1: System model with transform modulation and demodulation with quantization at both the transmitter and receiver. The transform modulation is modeled as a multiplication by V^H prior to quantization at the transmitter, while a spectrum analyzer and receiver employ the inverse transform V .

quantization [23], [25]–[28]. The AGN model has also been used in the analysis of low resolution mmWave systems [13]–[19]. In such systems, while the AGN and other Gaussian noise predictions match simulations, its use has not been rigorously justified.

This paper presents a simple, but rigorous method, for analyzing a large class of linear communication systems. Specifically, we analyze a general transmitter and receiver with quantization in conjunction with linear modulation and demodulation as shown in Fig. 1. A transmitter encodes data through an unitary transform V^H prior to the DAC. The DAC is modeled by a function $Q_{tx}(\cdot)$. The continuous-valued signal x is passed through a memoryless channel $F(\cdot)$. The receiver then uses an ADC $Q_{rx}(\cdot)$ followed by an inverse transform V to recover the transmitted symbols.

If V were an FFT-matrix, then the model can be considered as a simplified version of a frequency-domain filtering. Also, the spectrum of the transmitted signal can be modeled through the transform $r = Vx$. We find an achievable rate for this system and the power spectral density of the transmitted signal as a function of the DAC and ADC functions in a certain large random limit where $V \in \mathbb{C}^{N \times N}$ is selected uniformly among the unitary matrices and $N \rightarrow \infty$. We also find a capacity upper bound for a given transmitted power spectral density considering the DAC and the ADC, but not limiting transmit/receive processing to linear operations. Our key results are as follows:

- *Rigorous AGN model:* We show that the effect of quantization can be precisely modeled as additive, independent Gaussian noise. This result makes the AGN analysis of [23] in the setting of Fig. 1 rigorous, even in the low rate regime.
- *Predictions on the rate and power spectrum:* The AGN model provides asymptotically exact, simple and intuitive expressions for spectrum of the transmitted signal and a lower bound for the capacity of the quantized channel.
- *Sampling rate and spectral modeling:* Many prior information theoretic analyses of low-resolution communication systems assume that the symbol rate equals the sample rate (see, for example, [8], [13]). However, almost all practical transceivers use a sampling rate higher than the signal bandwidth to reduce the filtering requirements in the analog domain. Oversampling is also needed in systems with variable bandwidths where sub-channels are selected digitally (see Sec. V for an example based on 5G New Radio standard [29]). Previous works accounting for oversampling consider very specific up-sampling methods [30]. In contrast, our methods enable exact calculations of the power spectrum and bounds on capacity under general spectral mask constraints.
- *Implications for fully-digital architectures for 5G New Radio:* Several prior simulation studies have predicted that with 3 – 4 bits, the loss from quantization in achievable rate is minimal for data and control plane operations in most 5G cellular use cases [1]–[3], [7], [12], [16]–[19]. Our analysis provides a rigorous confirmation of this minimal loss in achievable rate. However, we also show that simple linear modulation results in a hard limit on the degree to which the out-of-band (OOB) noise can be suppressed. This OOB noise is, in fact, much more of an issue that the rate loss at most practical parameter values in 5G systems today, particularly in licensed spectrum deployments where adjacent carrier leakage is strictly limited.
- *Upper bounds on OOB suppression for any transmitter:* The high OOB levels with the simple linear modulator raises the question if there are any transmitter (possibly non-linear) that can provide greater OOB suppression. Interestingly, our capacity upper bound for a given power spectral density closely matches the achievable rate by the linear transform transmitter in some regime, but shows possibility for greater OOB suppression in other regimes.

A full version of this paper can be found in [31] that includes all proofs.

II. SYSTEM MODEL

A. Transceiver with Transform Modulation and Demodulation

We consider the general transceiver system with quantization and transform modulation and demodulation shown in Fig. 1. The transmitter constructs a vector of N symbols $\mathbf{z} = (z_0, \dots, z_{N-1})$ which are modulated as $\mathbf{u} = \mathbf{V}^H \mathbf{z}$ where $\mathbf{V} \in \mathbb{C}^{N \times N}$ is some unitary matrix. The transformed

values are quantized to result in a transmitted vector $\mathbf{x} = \mathbf{Q}_{\text{tx}}(\mathbf{u}) = \mathbf{Q}_{\text{tx}}(\mathbf{V}^H \mathbf{z})$, where $\mathbf{Q}_{\text{tx}}(\cdot)$ models the DAC. If \mathbf{V} were an FFT matrix, we could consider the symbols \mathbf{z} as the values of the transmitted signal in frequency domain and \mathbf{u} the pre-quantized values in time-domain. The modulation can thus be regarded as a simplified version of OFDM (where we ignore the cyclic prefix). In addition, if we zero-pad the input frequency-domain symbols \mathbf{z} , the transformed vector $\mathbf{u} = \mathbf{V}^H \mathbf{z}$ can be seen as an linearly up-sampled version of \mathbf{z} .

The transmitted time-domain symbols are passed through a general channel of the form,

$$\mathbf{y} = \mathbf{F}(\mathbf{x}, \boldsymbol{\xi}), \quad (1)$$

where $\mathbf{F}(\cdot)$ is some mapping and $\boldsymbol{\xi}$ is noise independent of the channel input \mathbf{x} . Most commonly, we will be interested in the AWGN case, $\mathbf{y} = h\mathbf{x} + \boldsymbol{\xi}$, where h is the channel gain. The channel (1) can also model certain non-linearities in the RF front-end [3]. The receiver first passes the signal through an ADC $\mathbf{Q}_{\text{rx}}(\mathbf{y})$ and then performs the inverse transform operation to obtain $\hat{\mathbf{z}} = \mathbf{V} \mathbf{Q}_{\text{rx}}(\mathbf{y})$.

B. Spectrum and Capacity

We are interested in estimating the effect of quantization on two key quantities: the frequency-domain *power spectrum* and the *capacity*.

To model the spectrum, let $\mathbf{r} = \mathbf{V}\mathbf{x}$ which is the transform of the transmitted signal \mathbf{x} . The component $|r_k|^2$ can be regarded as the energy of the signal at frequency $k, k = 0, \dots, N-1$. We assume the frequency is divided into M sub-bands and let $a_k \in \{1, \dots, M\}$ be the variable that indicates which sub-band frequency k belongs to. We call $\mathbf{a} = (a_0, \dots, a_{N-1})$ the *sub-band selection vector* and let,

$$\delta_m(\mathbf{a}) := \frac{1}{N} \sum_{k=0}^{N-1} \mathbb{1}_{\{a_k=m\}}, \quad (2)$$

which represents the fraction of the frequency components in sub-band m . We also define,

$$\phi_m(\mathbf{r}) := \frac{1}{N} \sum_{k=0}^{N-1} \mathbb{1}_{\{a_k=m\}} |r_k|^2, \quad (3)$$

which represents the energy per sample in sub-band m .

An achievable rate for the system can be computed by fixing some distribution on \mathbf{z} and computing the mutual information $I(\mathbf{z}; \hat{\mathbf{z}})$ between the transmitted vectors \mathbf{z} and received frequency-domain vectors, $\hat{\mathbf{z}}$. For the input distribution, we will use an independent complex Gaussian in each frequency. Specifically, we will assume the components z_k are independent with,

$$z_k \sim \mathcal{CN}(0, P_m) \text{ when } a_k = m, \quad (4)$$

where P_m is the symbol energy on any component in sub-band m . The average per symbol energy is,

$$\bar{P} = \frac{1}{N} \mathbb{E} \|\mathbf{z}\|^2 = \frac{1}{N} \mathbb{E} \|\mathbf{u}\|^2 = \sum_{m=1}^M \delta_m P_m, \quad (5)$$

where δ_m are the bandwidth fractions (2).

III. ACHIEVABLE SPECTRAL ENERGY AND RATE

A. Large System Limit

To make the analysis tractable, we consider a certain large system limit of random instances of the system indexed by the dimension N with $N \rightarrow \infty$. For each N , instead of considering the deterministic FFT matrix \mathbf{V} , we suppose that $\mathbf{V} = \mathbf{V}(N)$ is a random unitary matrix that is uniformly distributed on the $N \times N$ unitary matrices i.e., Haar distributed. The sub-band selection vectors $\mathbf{a} = \mathbf{a}(N)$ are assumed to be a deterministic sequence satisfying,

$$\lim_{N \rightarrow \infty} \frac{1}{N} |\{a_k(N) = m\}| = \delta_m. \quad (6)$$

The condition (6) imposes that asymptotically a fraction δ_m of the components are in sub-band m .

For the DAC function, $\mathbf{Q}_{\text{tx}}(\mathbf{u})$, we require that it is Lipschitz continuous and *componentwise separable* (or, equivalently memoryless operation) meaning that

$$\mathbf{x} = \mathbf{Q}_{\text{tx}}(\mathbf{u}) \iff x_n = Q_{\text{tx}}(u_n), \quad (7)$$

for some scalar-input, scalar-output function $Q_{\text{tx}}(\cdot)$. The componentwise function $Q_{\text{tx}}(\cdot)$ does not change with N . Similarly, we assume that the channel $\mathbf{F}(\cdot)$ and receiver ADC function act componentwise with Lipschitz functions $F(\cdot)$ and $Q_{\text{rx}}(\cdot)$. This corresponds to a memoryless channel. Typical quantizers are not Lipschitz continuous, but they can be approximated arbitrarily closely by a Lipschitz function. We will validate through simulations in Sec. V that our predictions hold true even for standard discontinuous quantizers.

B. Achievable Spectral Energy Distributions

We first compute the asymptotic power spectral distribution of the transmitted symbols \mathbf{x} . We define:

$$\alpha_{\text{tx}} := \frac{1}{P} \mathbb{E} [Q_{\text{tx}}^*(U)U], \quad \tau_{\text{tx}} := \frac{1}{P} \mathbb{E} |Q_{\text{tx}}(U) - \alpha_{\text{tx}}U|^2, \quad (8)$$

where \bar{P} is the average per symbol energy in \mathbf{z} in (5), $Q_{\text{tx}}^*(U)$ is the complex conjugate of $Q_{\text{tx}}(U)$ and the expectation in (8) is over $U \sim \mathcal{CN}(0, \bar{P})$.

Theorem 1. *Under the above assumptions, let $\mathbf{r} = \mathbf{V}\mathbf{x}$ be the frequency-domain representation of the transmitted signal \mathbf{x} . Then the energy in each sub-band converges almost surely to,*

$$\begin{aligned} s_m &:= \lim_{N \rightarrow \infty} \frac{1}{N} \sum_{k=0}^{N-1} |r_k|^2 \mathbb{1}_{\{a_k=m\}} \\ &= \delta_m [|\alpha_{\text{tx}}|^2 P_m + \tau_{\text{tx}} \bar{P}]. \end{aligned} \quad (9)$$

In particular, the total energy per symbol converges almost surely as,

$$s_{\text{tot}} := \lim_{N \rightarrow \infty} \frac{1}{N} \|\mathbf{x}\|^2 = (|\alpha_{\text{tx}}|^2 + \tau_{\text{tx}}) \bar{P}. \quad (10)$$

Proof. See Appendix C. \square

The proof of Theorem 1 shows, in fact, that the frequency-domain representation of the transmitted symbols can be written as

$$\mathbf{r} = \mathbf{V}\mathbf{x} = \alpha_{\text{tx}}\mathbf{z} + \mathbf{w}_{\text{tx}}, \quad (11)$$

where \mathbf{w}_{tx} has components that are asymptotically independent of \mathbf{z} and “Gaussian-like” with distribution $\mathcal{CN}(0, \tau_{\text{tx}}\bar{P})$. The vector \mathbf{w}_{tx} can be thought as the transmitter quantization noise. The precise sense in which \mathbf{w}_{tx} is Gaussian-like is given is somewhat technical and given in the Appendix. What is relevant is that the effect of quantizing and returning to frequency domain has the effect of scaling the signal \mathbf{z} and adding Gaussian noise. This makes precise the AGN model in [23], [24] used in several prior analyzes of low-resolution digital architectures [7], [12].

From Theorem 1, we see that the fraction of power in sub-band m is,

$$\nu_m := \frac{s_m}{s_{\text{tot}}} = \frac{\delta_m (|\alpha_{\text{tx}}|^2 P_m / \bar{P} + \tau_{\text{tx}})}{|\alpha_{\text{tx}}|^2 + \tau_{\text{tx}}}. \quad (12)$$

For a given DAC function $Q_{\text{tx}}(\cdot)$ and input power level \bar{P} , it is shown in Appendix D that there exists power levels P_m resulting in an energy fraction vector $\boldsymbol{\nu} = (\nu_1, \dots, \nu_M)$ if and only if $\nu_m \geq 0$, $\sum_m \nu_m = 1$ and

$$\nu_m \geq \frac{\delta_m \tau_{\text{tx}}}{|\alpha_{\text{tx}}|^2 + \tau_{\text{tx}}}. \quad (13)$$

We will call the set of $\boldsymbol{\nu}$ satisfying these constraints *linear feasible set*. Note that (13) shows there is a lower bound on the energy in any sub-band. This arises, intuitively, from the fact that the quantization noise is white and places energy across the spectrum. We will see below that this results in high OOB emissions settings where the sampling rate is higher than the signal bandwidth.

C. Achievable Rate

We next compute the asymptotic achievable rate given by the per symbol mutual information between the transmitted symbols \mathbf{z} and received symbols $\hat{\mathbf{z}}$:

$$R_{\text{lin}} := \liminf_{N \rightarrow \infty} \frac{1}{N} I(\mathbf{z}; \hat{\mathbf{z}}), \quad (14)$$

We will call this the *linear rate*, since it would be the rate achievable by the linear transmitter and receiver in Fig. 1. Assuming the components of the noise ξ_n are i.i.d. with some distribution $\xi_n \sim \Xi$ with $\mathbb{E}|\Xi|^2 < \infty$, similar to (8), we define

$$\alpha_{\text{rx}} := \frac{1}{P} \mathbb{E} [S^*U], \quad \tau_{\text{rx}} := \frac{1}{P} \mathbb{E} |S - \alpha_{\text{rx}}U|^2, \quad (15)$$

where S is the complex random variable,

$$S = Q_{\text{rx}}(F(Q_{\text{tx}}(U), \Xi)), \quad U \sim \mathcal{CN}(0, \bar{P}), \quad (16)$$

S^* is the complex conjugate of S , and U is independent of Ξ .

Theorem 2. *Under the above assumptions, the linear rate is almost surely bounded below by,*

$$R_{\text{lin}} \geq \sum_{m=1}^M \delta_m \log \left(1 + \frac{|\alpha_{\text{rx}}|^2 P_m}{\tau_{\text{rx}} \bar{P}} \right). \quad (17)$$

Proof. See Appendix E. \square

The rate has a simple interpretation. It is shown in Appendix E that the received symbols are given by,

$$\hat{\mathbf{z}} = \alpha_{\text{rx}} \mathbf{z} + \mathbf{w}_{\text{rx}}, \quad (18)$$

where \mathbf{w}_{rx} is asymptotically independent of \mathbf{z} and “Gaussian-like” with components $\mathcal{CN}(0, \tau_{\text{rx}} \bar{P})$ and can be seen as representing the combined effect of the noise in the channel as well as the DAC and ADC quantization noise. Similar to Theorem 1, the precise sense in which \mathbf{w}_{rx} is asymptotically Gaussian is given in the proof. Since \mathbf{z} has power P_m in sub-band m , the rate lower bound (17) is simply the Gaussian capacity under the AWGN model (18). Note that the presented lower bound is achieved using Gaussian inputs. However, as we will show in Sec. IV, using Gaussian inputs is not optimal since it does not achieve the maximum high SNR rate. Finding the optimal input distribution is left for future work.

D. Achievable Rate in an AWGN Channel

It is useful to consider the special case when we have an additive white Gaussian noise (AWGN) channel modeled with the function $F(X, \Xi) = X + \Xi$ and $\Xi \sim \mathcal{CN}(0, \sigma^2)$. Also, to make the calculations simple, suppose we assume there is no quantization at the receiver so that $Q_{\text{rx}}(y_n) = y_n$. Substituting these distributions into (15), and using the expressions in (8), we can show that

$$\alpha_{\text{rx}} = \alpha_{\text{tx}}, \quad \tau_{\text{rx}} = \tau_{\text{tx}} + \frac{\sigma^2}{\bar{P}}. \quad (19)$$

Substituting these values into (17), we obtain,

$$R_{\text{lin}} \geq \sum_{m=1}^M \delta_m \log \left(1 + \frac{|\alpha_{\text{tx}}|^2 P_m}{\tau_{\text{tx}} \bar{P} + \sigma^2} \right). \quad (20)$$

Hence we get the AWGN capacity with a loss from the DAC quantization noise.

E. Achievable Rate When There is No Noise

We now consider the noise-free case.

Theorem 3. *In an AWGN channel if $\sigma^2 = 0$, then the rate bound in (20) is given by,*

$$R_{\text{lin}} \geq \log \left(1 + \frac{|\alpha_{\text{tx}}|^2}{\tau_{\text{tx}}} \right) - D(\delta \| \nu), \quad (21)$$

for any set of power distributions ν_m is given by (12).

Proof. See Appendix F. \square

Even with no noise, the rate is finite since linear processing results in Gaussian-like quantization noise. Also, the linear rate in (21) is only achievable for feasible power allocations (13).

The rate bound (21) has an interesting interpretation. The first term on the right hand side of (21), $\log(1 + |\alpha_{\text{tx}}|^2 / \tau_{\text{tx}})$, is the rate in (20) if the energies in the sub-bands were allocated evenly, $P_m = \bar{P}$ for all m . Also, observe that from (12), when $P_m = \bar{P}$, $\nu_m = \delta_m$. So the case of $\nu = \delta$ corresponds

to the equal power allocation case. The second term, $D(\delta \| \nu)$, in the right hand side of (21) is a measure of the loss as a result of non-uniformly allocating the power. In particular, if one attempts to reduce the power in some sub-band (e.g. it is an adjacent carrier), there will be a linear modulation rate penalty.

IV. QUANTIZED CAPACITY UPPER BOUND

The results above show that a linear transceiver in conjunction with quantization limits system performance in two key ways: (a) there is a limit (13) to which OOB emissions can be suppressed; and (b) even in the regimes in which a desired spectral mask is feasible, there is a rate penalty due to quantization noise. These shortcomings raise the question of whether there are transceivers (possibly non-linear) that can achieve better rate under quantization constraints. To understand this, consider again transmitting on N complex symbols, $\mathbf{x} = (x_0, \dots, x_{N-1})$. Model the DAC constraint as a constraint, $x_n \in A$ where $A \subset \mathbb{C}$ are the possible values of the (complex) DAC. We will write this constraint as,

$$\mathbf{x} \in A^N := \{\mathbf{x} \mid x_n \in A\}, \quad (22)$$

To impose the spectral mask constraints, let $\mathbf{s} = (s_1, \dots, s_M)$ be a vector of target energies in each sub-band. Recall that $\phi_m(\mathbf{V}\mathbf{x})$ in (3) is the energy in a sub-band for a transmitted vector \mathbf{x} . Thus, the set

$$G_N(\mathbf{V}, \epsilon) := \{\mathbf{x} \in A^N \mid \phi_m(\mathbf{V}\mathbf{x}) \in [s_m - \epsilon, s_m] \forall m\}, \quad (23)$$

represents the set of vectors \mathbf{x} satisfying the DAC constraint and the sub-band energy constraints within some tolerance $\epsilon > 0$. If we restrict the modulation to vectors in the set $G_N(\mathbf{V}, \epsilon)$, then the maximum rate any modulation method can obtain is,

$$R_N(\mathbf{V}, \epsilon) := \frac{1}{N} \log |G_N(\mathbf{V}, \epsilon)|, \quad (24)$$

where $|G_N(\mathbf{V}, \epsilon)|$ is the cardinality of $G_N(\mathbf{V}, \epsilon)$.

As before, assume $\mathbf{V} \in \mathbb{C}^{N \times N}$ is Haar-distributed on the unitary matrices. Since \mathbf{V} is random, the rate $R_N(\mathbf{V}, \epsilon)$ in (24) is also random. We can use Jensen's inequality to upper bound the expected rate,

$$\mathbb{E} R_N(\mathbf{V}, \epsilon) = \frac{1}{N} \mathbb{E} \log |G_N(\mathbf{V}, \epsilon)| \leq \frac{1}{N} \log \mathbb{E} |G_N(\mathbf{V}, \epsilon)|.$$

Here, the expectation is over \mathbf{V} . We will be interested in the asymptotic value of this upper bound,

$$\bar{R} := \lim_{\epsilon \rightarrow 0} \lim_{N \rightarrow \infty} \frac{1}{N} \log \mathbb{E} |G_N(\mathbf{V}, \epsilon)|. \quad (25)$$

In this definition, we take the limit $\epsilon \rightarrow 0$ to ensure that the modulator asymptotically matches the target sub-band energy levels exactly. Note that the order of the limits over N and ϵ is important.

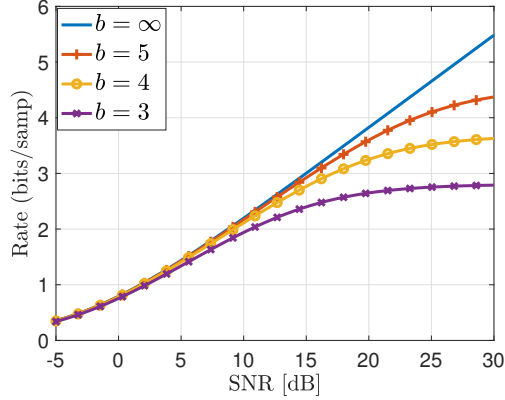


Fig. 2: Achievable rate of a system where all the transmit power is allocated to one of two sub-band for different number of DAC bits.

Theorem 4. Let $\mathbf{s} = (s_1, \dots, s_M)$ be a set of target sub-band energy levels. We define s_{tot} as the total energy, and $\boldsymbol{\nu} = (\nu_1, \dots, \nu_M)$ as the vector of energy distributions

$$s_{\text{tot}} := \sum_{m=1}^M s_m, \quad \nu_m = \frac{s_m}{s_{\text{tot}}}. \quad (26)$$

Then, under the above assumptions, the asymptotic rate upper bound in (25) is given by,

$$\bar{R} = H_{\max}(s_{\text{tot}}) - D(\boldsymbol{\delta} \parallel \boldsymbol{\nu}). \quad (27)$$

Here $H_{\max}(s)$ is given by

$$H_{\max}(s) = \max_V H(V) \text{ s.t. } \mathbb{E}|V|^2 = s, \quad (28)$$

where the maximization is over all discrete random variables V on the set A with second moment $\mathbb{E}|V|^2 = s$.

The rate upper bound in (27) has a natural interpretation. The term $H_{\max}(s_{\text{tot}})$ is the maximum entropy we could obtain if we are restricted to the DAC constellation A and need to achieve a certain total power s_{tot} . If we select the symbols of x_n from the distribution that achieves this entropy, we would obtain an output spectrum that is flat. If we need to have a non-uniform power spectrum, we pay an additional penalty $D(\boldsymbol{\delta} \parallel \boldsymbol{\nu})$. The term $D(\boldsymbol{\delta} \parallel \boldsymbol{\nu})$ is precisely the power distribution loss we saw in the linear rate lower bound (21). Note that as in Theorem 3, Theorem 4 applies to the no-noise case. Comparing the rate lower and upper bounds in these theorems, we see that there is a gap,

$$\bar{R} - R_{\text{lin}} \leq H_{\max}(s_{\text{tot}}) - \log \left(1 + \frac{|\alpha_{\text{tx}}|^2}{\tau_{\text{tx}}} \right). \quad (29)$$

We will see in the simulations below that for most practical values, this gap is less than one bit.

V. NUMERICAL RESULTS

To illustrate the results, consider a system where the transmission bandwidth is divided into two equal sub-bands of normalized widths $\delta_1 = \delta_2 = 0.5$. The base-band signal \mathbf{u}

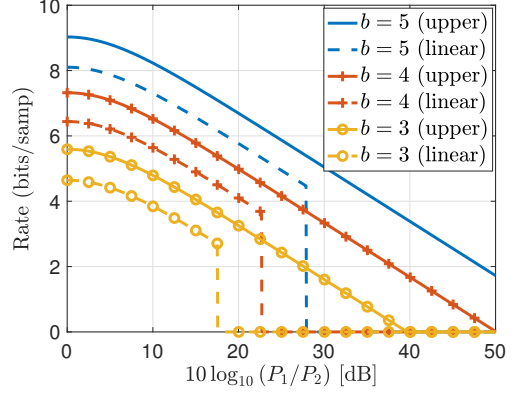


Fig. 3: Rate versus adjacent channel leakage in a two sub-band system. The solid lines show the upper bounds on the achievable rate (Theorem 4) and the dashed lines show the achievable rate predicted by the linear AGN model (Theorem 3).

is designed such that all its energy is concentrated over the first sub-band (representing an in-band signal). Any leakage into sub-band 2 (representing an adjacent band) is undesirable. Most wireless standard specify a minimum ratio of the in-band to the adjacent band power which defines the *spectrum mask*. The transmitter is equipped with a b -bit DAC. The finite resolution of the DAC introduces quantization noise both in-band and in the adjacent carrier.

The effect of the quantization noise on the in-band signal is shown in Fig. 2. The achievable rate over an AWGN channel for different SNRs and DAC resolutions (b) is computed using (20) assuming a scalar uniform quantizer in both real and imaginary components (I and Q). We observe that as the resolution of the DAC increases the achievable rate of the system becomes closer to the ideal AWGN capacity (i.e., $b = \infty$). Note that the high SNR achievable rate approaches b bits per sample instead of $2b$ (b bits from in-phase and b bits from quadrature components) since half of the bandwidth is used due to spectral mask constraints. More interestingly, we see that in the low SNR regime there is very little or no loss in rate due to low resolution quantizers. Practical mmWave systems generally operate at the low SNR range [12], particularly when SNR is achieved with beamforming. The results thus confirm that the rate loss will be negligible in typical low-SNR cellular settings as observed in extensive simulations mentioned earlier [7]–[10], [13]–[19].

On the other hand, a more serious issue is the spectral mask constraint. Fig. 3 plots the no-noise achievable rate from (21) as a function of the signal to adjacent power, P_1/P_2 , sometimes called the adjacent carrier leakage ratio (ACLR). We see that, with linear modulation, the maximum ACLR with non-zero rate is strictly limited. Fig. 3 also plots the theoretical maximum rate vs. ACLR from Theorem 4. In the feasible regime, the linear rate is within one bit of this upper bound. But, the upper bound at least permits higher ACLRs suggesting that more advanced transmitters may be able to suppress OOB emissions further.

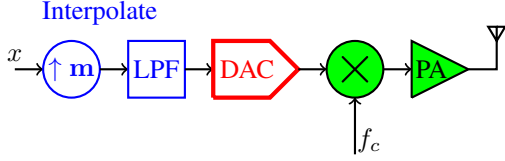


Fig. 4: Simplified diagram showing standard linear upconversion and transmission.

Practical low resolution 5G Systems: Our theory applies to a theoretical random transform model. We illustrate the model's predictive capabilities in a practical transceiver shown in in Fig. 4. We consider typical for multi-carrier operation in the 5G New Radio (NR) standard [29] using common parameters for 28 GHz [32]. To accommodate variable bandwidths, the DAC is typically run at a maximum sample rate. In this case, we assume an NR standard rate of $f_{\text{samp}} = 2 \times 491.5 = 983$ MHz. A mobile may be allocated a smaller bandwidth, say 200 MHz, which would be produced in the NR standard via an OFDM signal at 2×122.6 MHz. The modulated baseband signal would be then digitally upconverted to the sampling rate of f_{samp} MHz and digitally filtered to reject spectral images. This interpolated signal is passed through a b -bit DAC.

Fig. 5 shows the output power spectral density (PSD) under various numbers of bits in the DAC. We see that the low DAC resolution creates quantization noise across the entire bandwidth. The level of that noise increases as the DAC resolution (b) is lowered. Moreover, the OOB noise has a flat spectrum (with some decay due to the zero order hold circuit) and justifies the Gaussian model in (11).

Next, Fig. 6 shows the ratio of the in-band power (P_1) to the power “leaked” into the adjacent band (P_2) and compares the simulated system with linear AGN model in Theorem 1. We see that the AGN model is within ≈ 1 dB of the simulated adjacent channel leakage ratio. The error comes from the fact that the practical simulation models a zero order hold circuit which attenuates some of the OOB noise. Further, the NR OFDM specifications includes a guard band (≈ 10 MHz) which is not included in the theoretical calculations. Otherwise, we see that the theoretical model provides an excellent prediction of the spectrum in a practical low-resolution transmitter.

VI. CONCLUSIONS AND FUTURE WORK

We have presented a simple large random limit model for analyzing the effect of quantization on a class of linear transceivers. Importantly, the analysis rigorously captures both the effects on rate and power spectrum, including OOB emissions – key properties for emerging mmWave systems. The analysis confirms earlier simulations that, for 5G systems, low-resolution transceivers cause negligible loss in achievable communication rates. However, OOB emissions are more problematic. From an information theoretic perspective, this motivates consideration of more advanced modulation and demodulation methods used in conjunction with low resolution DAC and ADC. An obvious class of methods would be

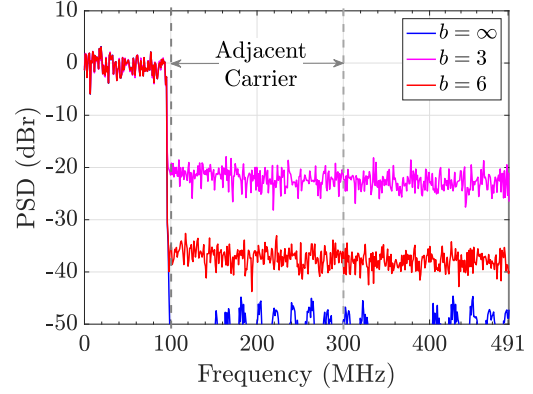


Fig. 5: PSD of the linear modulator used for transmitting a 400 MHz channel centered at 28 GHz in a 5G NR system sample rate $f_{\text{samp}} = 983$ Ms/s. The PSD is shown for various number of bits (n) in the DAC.

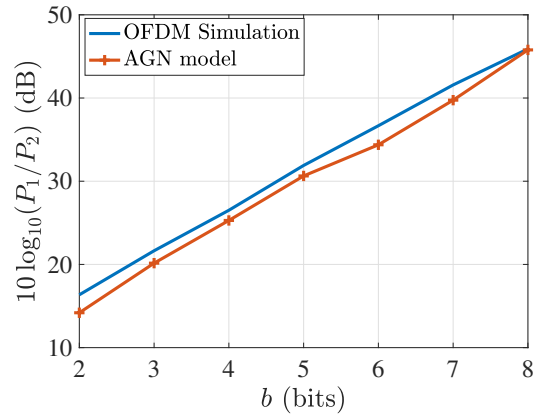


Fig. 6: ACLR with a finite DAC resolution (b) for a 200 MHz 3GPP NR OFDM transmitter compared with the proposed AGN model.

approximate message passing (AMP) algorithms designed for systems with random unitary transforms [33]–[38]. These methods indeed have already been used in mmWave low-resolution receivers [39]. In addition, improved bounds similar to Theorem 4 can likely be derived from related statistical physical techniques that analyze systems exactly of this form [40], [41].

REFERENCES

- [1] W. B. Abbas, F. Gomez-Cuba, and M. Zorzi, “Millimeter wave receiver efficiency: A comprehensive comparison of beamforming schemes with low resolution ADCs,” *IEEE Trans. Wireless Commun.*, vol. 16, no. 12, pp. 8131–8146, Dec. 2017.
- [2] J. Zhang *et al.*, “On low-resolution ADCs in practical 5G millimeter-wave massive MIMO systems,” *IEEE Commun. Mag.*, vol. 56, no. 7, pp. 205–211, Jul. 2018.
- [3] M. Abdelghany *et al.*, “Towards all-digital mmWave massive MIMO: Designing around nonlinearities,” in *Proc. IEEE Asilomar Conf. Signals, Syst., Comput.*, 2018, pp. 1552–1557.
- [4] A. Khalili *et al.*, “Tradeoff between delay and high SNR capacity in quantized MIMO systems,” in *Proc. IEEE Int. Symp. Inf. Theory*, pp. 597–601, Jul. 2019.

- [5] —, “On multiterminal communication over MIMO channels with one-bit ADCs at the receivers,” *Proc. IEEE Int. Symp. Inf. Theory*, pp. 602–606, Jul. 2019.
- [6] —, “On throughput of millimeterwave MIMO systems with low resolution ADCs,” *Proc. IEEE Int. Conf. on Acoustics, Speech and Signal Processing (ICASSP)*, pp. 5255–5259, 2020.
- [7] C. N. Barati *et al.*, “Initial access in millimeter wave cellular systems,” *IEEE Trans. Wireless Commun.*, vol. 15, no. 12, pp. 7926–7940, Dec. 2016.
- [8] J. Singh, O. Dabeer, and U. Madhow, “On the limits of communication with low-precision analog-to-digital conversion at the receiver,” *IEEE Trans. Commun.*, vol. 57, no. 12, pp. 3629–3639, Dec. 2009.
- [9] T. Koch and A. Lapidoth, “At low SNR, asymmetric quantizers are better,” *IEEE Trans. Inf. Theory*, vol. 59, no. 9, pp. 5421–5445, Sept. 2013.
- [10] J. A. Nossek and M. T. Ivrlač, “Capacity and coding for quantized MIMO systems,” in *Proc. Intl. Conf. Wireless Commun. and Mobile Comput.*, 2006, pp. 1387–1392.
- [11] O. Orhan, E. Erkip, and S. Rangan, “Low power analog-to-digital conversion in millimeter wave systems: Impact of resolution and bandwidth on performance,” in *Proc. IEEE Inf. Theory Appl. Wkshp. (ITA)*, 2015, pp. 191–198.
- [12] S. Dutta *et al.*, “A case for digital beamforming at mmWave,” *IEEE Trans. Wireless Commun.*, vol. 19, no. 2, pp. 756–770, Feb. 2020.
- [13] J. Mo and R. W. Heath, “Capacity analysis of one-bit quantized MIMO systems with transmitter channel state information,” *IEEE Trans. Signal Process.*, vol. 63, no. 20, pp. 5498–5512, Oct. 2015.
- [14] S. Rini *et al.*, “A general framework for low-resolution receivers for MIMO channels,” *arXiv preprint arXiv:1702.08133*, 2017.
- [15] A. Mezghani and J. A. Nossek, “Capacity lower bound of MIMO channels with output quantization and correlated noise,” in *Proc. IEEE Int. Symp. Inf. Theory*, 2012, pp. 1–5.
- [16] C. Studer and G. Durisi, “Quantized massive MU-MIMO-OFDM uplink,” *IEEE Trans. Commun.*, vol. 64, no. 6, pp. 2387–2399, Jun. 2016.
- [17] S. Jacobsson *et al.*, “Throughput analysis of massive MIMO uplink with low-resolution ADCs,” *IEEE Trans. Wireless Commun.*, vol. 16, no. 6, pp. 4038–4051, Jun. 2017.
- [18] C. Mollen *et al.*, “Uplink performance of wideband massive MIMO with one-bit ADCs,” *IEEE Trans. Wireless Commun.*, vol. 16, no. 1, pp. 87–100, Jan. 2016.
- [19] J. Mo *et al.*, “Hybrid architectures with few-bit ADC receivers: Achievable rates and energy-rate tradeoffs,” *IEEE Trans. Wireless Commun.*, vol. 16, no. 4, pp. 2274–2287, Apr. 2017.
- [20] T. S. Rappaport *et al.*, *Millimeter wave wireless communications*. Pearson Education, 2014.
- [21] S. Rangan, T. S. Rappaport, and E. Erkip, “Millimeter-wave cellular wireless networks: Potentials and challenges,” *Proceedings of the IEEE*, vol. 102, no. 3, pp. 366–385, Mar. 2014.
- [22] A. Khalili *et al.*, “On MIMO channel capacity with output quantization constraints,” *Proc. IEEE Int. Symp. Inf. Theory*, pp. 1355–1359, Jun. 2018.
- [23] A. Gersho and R. M. Gray, *Vector quantization and signal compression*. Springer Science & Business Media, 2012, vol. 159.
- [24] A. K. Fletcher *et al.*, “Robust predictive quantization: Analysis and design via convex optimization,” *IEEE J. Sel. Topics Signal Process.*, vol. 1, no. 4, pp. 618–632, Dec. 2007.
- [25] D. Marco and D. L. Neuhoff, “The validity of the additive noise model for uniform scalar quantizers,” *IEEE Trans. Inf. Theory*, vol. 51, no. 5, pp. 1739–1755, May 2005.
- [26] R. M. Gray and T. G. Stockham, “Dithered quantizers,” *IEEE Trans. Inf. Theory*, vol. 39, no. 3, pp. 805–812, May 1993.
- [27] R. Zamir and M. Feder, “On lattice quantization noise,” *IEEE Trans. Inf. Theory*, vol. 42, no. 4, pp. 1152–1159, Jul. 1996.
- [28] M. S. Derpich, J. Østergaard, and G. C. Goodwin, “The quadratic Gaussian rate-distortion function for source uncorrelated distortions,” in *Proc. Data Compression Conf. (DCC)*, 2008, pp. 73–82.
- [29] 3GPP TS 38.300, “NR and NG-RAN overall description; stage 2,” 2020, v15.3.1.
- [30] S. Krone and G. Fettweis, “Fading channels with 1-bit output quantization: Optimal modulation, ergodic capacity and outage probability,” in *Proc. IEEE Inf. Theory Wkshp.*, 2010, pp. 1–5.
- [31] S. Dutta *et al.*, “Capacity bounds for communication systems with quantization and spectral constraints,” *arXiv preprint arXiv:2001.03870*, 2020.
- [32] 3GPP, “TS 38.104, Base station (BS) radio transmission and reception,” 2019.
- [33] J. Ma and L. Ping, “Orthogonal AMP,” *IEEE Access*, vol. 5, pp. 2020–2033, 2017.
- [34] S. Rangan, P. Schniter, and A. K. Fletcher, “Vector approximate message passing,” *IEEE Trans. Inf. Theory*, pp. 6664–6684, Oct. 2019.
- [35] B. Cakmak, O. Winther, and B. H. Fleury, “S-AMP: Approximate message passing for general matrix ensembles,” in *Proc. IEEE Inf. Theory Wkshp.*, 2014, pp. 192–196.
- [36] A. K. Fletcher, S. Rangan, and P. Schniter, “Inference in deep networks in high dimensions,” in *Proc. IEEE Int. Symp. Inf. Theory*, 2018, pp. 1884–1888.
- [37] P. Schniter, S. Rangan, and A. K. Fletcher, “Vector approximate message passing for the generalized linear model,” in *Proc. IEEE Asilomar Conf. Signals, Syst., Compute.*, 2016, pp. 1525–1529.
- [38] H. He, C.-K. Wen, and S. Jin, “Generalized expectation consistent signal recovery for nonlinear measurements,” in *Proc. IEEE Int. Symp. Inf. Theory*, 2017, pp. 2333–2337.
- [39] J. Mo, P. Schniter, and R. W. Heath, “Channel estimation in broadband millimeter wave MIMO systems with few-bit ADCs,” *IEEE Trans. on Signal Process.*, vol. 66, no. 5, pp. 1141–1154, Mar. 2017.
- [40] G. Reeves, “Additivity of information in multilayer networks via additive Gaussian noise transforms,” in *Proc. Annual Allerton Conf. on Commun., Control, and Comput.*, 2017, pp. 1064–1070.
- [41] J. Barbier *et al.*, “Optimal errors and phase transitions in high-dimensional generalized linear models,” *Proc. National Academy of Sciences*, vol. 116, no. 12, pp. 5451–5460, Mar. 2019.
- [42] M. Bayati and A. Montanari, “The dynamics of message passing on dense graphs, with applications to compressed sensing,” *IEEE Trans. Inf. Theory*, vol. 57, no. 2, pp. 764–785, 2011.
- [43] A. Dembo and O. Zeitouni, *Large Deviations Techniques and Applications*. Springer, 2010.

APPENDIX A

EMPIRICAL CONVERGENCE OF RANDOM VARIABLES

For the results in Section III, we need to first review some technical definitions on empirical convergence of random variables. The analysis framework was developed by Bayati and Montanari [42] and also used in the VAMP analysis of [34]. For a given $p \geq 1$, a map $\mathbf{g} : \mathbb{C}^d \rightarrow \mathbb{C}^r$ is called *pseudo-Lipschitz* of order p if

$$\|\mathbf{g}(\mathbf{r}_1) - \mathbf{g}(\mathbf{r}_2)\| \leq C\|\mathbf{r}_1 - \mathbf{r}_2\| (1 + \|\mathbf{r}_1\|^{p-1} + \|\mathbf{r}_2\|^{p-1}), \quad (30)$$

for some constant $C > 0$. Note that when $p = 1$, we obtain the standard definition of Lipschitz continuity.

Now suppose that for each N , $\mathbf{x}(N)$ is a block vector $\mathbf{x}(N) = (\mathbf{x}_1, \dots, \mathbf{x}_N)$ with components $\mathbf{x}_n \in \mathbb{C}^d$ for some fixed dimension d . Thus, the total length of the vector is Nd . Let $X \in \mathbb{C}^d$ be a random vector. We say that the components $\mathbf{x}(N)$ converge empirically to X with p -th order moments if

$$\lim_{N \rightarrow \infty} \frac{1}{N} \sum_{n=0}^{N-1} \phi(\mathbf{x}_n(N)) = \mathbb{E}[\phi(X)], \quad (31)$$

for all pseudo-Lipschitz functions of order p . Loosely speaking, the condition requires that the empirical distribution of the components of $\mathbf{x}(N)$ converge in distribution to the random variable X . The condition will be satisfied when \mathbf{x}_n are i.i.d. with distribution X . We will often drop the index N and write,

$$\lim_{N \rightarrow \infty} \{\mathbf{x}_n\} \stackrel{PL(p)}{=} X. \quad (32)$$

APPENDIX B

DISTRIBUTIONS UNDER RANDOM TRANSFORMS

We next need a key result from [34] that describes the distribution of vectors under random unitary transforms. Consider a sequence of systems indexed by N , and for each N suppose that $\mathbf{V} \in \mathbb{C}^{N \times N}$ is uniformly distributed on the unitary matrices. Let $(\mathbf{x}, \mathbf{s}) = (\mathbf{x}(N), \mathbf{s}(N))$ be a sequence of vectors that converge empirically to random variables (X, S) in that

$$\lim_{N \rightarrow \infty} \{(x_n, s_n)\} \stackrel{PL(2)}{=} (X, S). \quad (33)$$

Now consider a vector \mathbf{y} generated by,

$$\mathbf{y} = \mathbf{V}\phi(\mathbf{V}^H \mathbf{x}, \xi), \quad (34)$$

where $\phi(\cdot)$ is some function that operates componentwise in that

$$\mathbf{y} = \phi(\mathbf{z}, \xi) \iff y_n = \phi(z_n, \xi_n),$$

for some scalar-valued, Lipschitz-continuous function $\phi(\cdot)$. Assume that ξ also converges empirically in that

$$\lim_{N \rightarrow \infty} \{\xi_n\} \stackrel{PL(2)}{=} \Xi,$$

for some random variable Ξ . To analyze the statistics on \mathbf{y} , we define three key quantities:

$$P := \mathbb{E}|X|^2, \quad (35a)$$

$$\alpha := \frac{1}{P} \mathbb{E}(\overline{Z}\phi(Z, \Xi)), \quad (35b)$$

$$\tau_w := \frac{1}{P} \mathbb{E}|\phi(Z, \Xi) - \alpha Z|^2. \quad (35c)$$

where $Z \sim \mathcal{CN}(0, P)$.

Proposition 1. *Under the above assumptions, the components of $(\mathbf{y}, \mathbf{x}, \mathbf{s})$ converge empirically as,*

$$\lim_{N \rightarrow \infty} \{(y_n, x_n, s_n)\} \stackrel{PL(2)}{=} (Y, X, S), \quad (36)$$

where (X, S) are the random variables in (33) and

$$Y = \alpha X + W, \quad W \sim \mathcal{CN}(0, \tau_w P), \quad (37)$$

with W independent of (X, S) .

Proof. This is a special case of one iteration of the general convergence result in [34, Appendix D]. That work considers the real-valued case, but the complex case can be proven similarly. \square

The model (37) shows that transformation on \mathbf{x} to produce \mathbf{y} recovers a linearly scaled \mathbf{x} plus Gaussian noise. The scaling factor α and Gaussian noise variance τ_w can be computed from the distributions of the components.

APPENDIX C

PROOF OF THEOREM 1

The theorem is a direct application of the linear model in Proposition 1. To use the proposition, first observe that, due to (6) and the Gaussian distribution on \mathbf{z} in (4), we have that the sub-band selection \mathbf{a} and the frequency-domain inputs \mathbf{z} converge empirically as,

$$\lim_{n \rightarrow \infty} \{(z_n, a_n)\} \stackrel{PL(2)}{=} (Z, A), \quad (38)$$

where $A \in \{1, \dots, M\}$ is a discrete random variable with $\Pr(A = m) = \delta_m$ and Z is the conditional complex Gaussian,

$$Z \sim \mathcal{CN}(0, P_m) \text{ when } A = m.$$

In particular, the average energy of Z is,

$$\mathbb{E}|Z|^2 = \sum_{m=1}^M \delta_m P_m =: \overline{P}. \quad (39)$$

Now, the frequency domain components of the transmitted vector \mathbf{x} are given by,

$$\mathbf{r} = \mathbf{V}\mathbf{x} = \mathbf{V}\mathbf{Q}(\mathbf{V}^H \mathbf{z}).$$

Proposition 1 then shows that the components of $(\mathbf{r}, \mathbf{z}, \mathbf{a})$ converge empirically as,

$$\lim_{N \rightarrow \infty} \{(r_n, z_n, a_n)\} \stackrel{PL(2)}{=} (R, Z, A),$$

and

$$R = \alpha_{\text{tx}} Z + W_{\text{tx}}, \quad W_{\text{tx}} \sim \mathcal{CN}(0, \tau_{\text{tx}} \overline{P}),$$

where W_{tx} is independent of Z . The sub-band energies,

$$\begin{aligned} s_m &:= \lim_{N \rightarrow \infty} \sum_{k=0}^{N-1} |r_k|^2 \mathbb{1}_{\{a_k=m\}} \\ &= \mathbb{E} [|R|^2 \mathbb{1}_{\{A=m\}}] \\ &= \mathbb{E} [|\alpha_{\text{tx}} Z + W_{\text{tx}}|^2 | A = m] \Pr(A = m) \\ &= [|\alpha_{\text{tx}}|^2 P_m + \tau_{\text{tx}} \bar{P}] \delta_m. \end{aligned} \quad (40)$$

This proves (9). To prove (10),

$$\begin{aligned} s_{\text{tot}} &= \sum_{m=1}^M s_m = \sum_{m=1}^M [|\alpha_{\text{tx}}|^2 P_m + \tau_{\text{tx}} \bar{P}] \delta_m \\ &= (|\alpha_{\text{tx}}|^2 + \tau_{\text{tx}}) \bar{P}, \end{aligned}$$

where the last step used (39) and the fact that $\sum_m \delta_m = 1$.

APPENDIX D THE LINEAR RATE REGION

The following proposition shows that power allocations ν_m are feasible if and only if they satisfy (13).

Proposition 2. *Let $\alpha_{\text{tx}} \in \mathbb{C}$, $\tau_{\text{tx}} > 0$, $\bar{P} > 0$ and $\delta_m \geq 0$ with $\sum_m \delta_m = 1$ be given. For any $\boldsymbol{\nu} = (\nu_1, \dots, \nu_M)$, the following are equivalent:*

- (a) *There exists $P_m \geq 0$ such that $\bar{P} = \sum_m \delta_m P_m$ and ν_m is given by (12) for all m .*
- (b) *ν_m satisfies (13) for all m and $\sum_m \nu_m = 1$.*

Proof. (a) \Rightarrow (b): Suppose there exists $P_m \geq 0$ as in (a) and let ν_m be given by (12). Since $\bar{P} = \sum_m \delta_m P_m$, we have $\sum_m \nu_m = 1$. Also, since $P_m \geq 0$, we have ν_m in (12) satisfies the lower bound (13).

(b) \Rightarrow (a): Conversely, suppose we are given $\boldsymbol{\nu}$ satisfying (13) with $\sum_m \nu_m = 1$. Set,

$$P_m = \left[\frac{\nu_m}{\delta_m} (|\alpha_{\text{tx}}|^2 + \tau_{\text{tx}}) - \tau_{\text{tx}} \right] \frac{\bar{P}}{|\alpha_{\text{tx}}|^2}. \quad (41)$$

Therefore, ν_m satisfies (12). Since ν_m satisfies (13), P_m in (41) satisfies $P_m \geq 0$. Also,

$$\begin{aligned} \sum_m \delta_m P_m &= \frac{\bar{P}}{|\alpha_{\text{tx}}|^2} \left[\sum_m \nu_m (|\alpha_{\text{tx}}|^2 + \tau_{\text{tx}}) - \sum_m \delta_m \tau_{\text{tx}} \right] \\ &= \frac{\bar{P}}{|\alpha_{\text{tx}}|^2} [|\alpha_{\text{tx}}|^2 + \tau_{\text{tx}} - \tau_{\text{tx}}] = \bar{P}, \end{aligned}$$

where we have used the fact that $\sum_m \nu_m = 1$ and $\sum_m \delta_m = 1$. \square

APPENDIX E PROOF OF THEOREM 2

We need two basic mutual information lemmas. For $m = 1, \dots, M$, let $\mathbf{z}^{(m)}$ and $\hat{\mathbf{z}}^{(m)}$ denote the sub-vectors of \mathbf{z} and $\hat{\mathbf{z}}$ with components in sub-band m . That is,

$$\mathbf{z}^{(m)} = \{z_k | a_k = m\},$$

and $\hat{\mathbf{z}}^{(m)}$ is defined similarly.

Lemma 1. *The mutual information is bounded below by,*

$$I(\mathbf{z}; \hat{\mathbf{z}}) \geq \sum_{m=1}^M I(\mathbf{z}^{(m)}; \hat{\mathbf{z}}^{(m)}). \quad (42)$$

Proof. By the mutual information chain rule,

$$I(\mathbf{z}; \hat{\mathbf{z}}) \geq \sum_{m=1}^M I(\mathbf{z}^{(m)}; \hat{\mathbf{z}} | \mathbf{z}^{(1)}, \dots, \mathbf{z}^{(m-1)}). \quad (43)$$

Also, since the components \mathbf{z} are independent, the vectors $\mathbf{z}^{(m)}$ are independent for different m . Hence,

$$H(\mathbf{z}^{(m)} | \mathbf{z}^{(1)}, \dots, \mathbf{z}^{(m-1)}) = H(\mathbf{z}^{(m)}). \quad (44)$$

Therefore,

$$\begin{aligned} I(\mathbf{z}^{(m)}; \hat{\mathbf{z}} | \mathbf{z}^{(1)}, \dots, \mathbf{z}^{(m-1)}) &= H(\mathbf{z}^{(m)} | \mathbf{z}^{(1)}, \dots, \mathbf{z}^{(m-1)}) \\ &\quad - H(\mathbf{z}^{(m)} | \hat{\mathbf{z}}, \mathbf{z}^{(1)}, \dots, \mathbf{z}^{(m-1)}) \\ &\stackrel{(a)}{=} H(\mathbf{z}^{(m)}) - H(\mathbf{z}^{(m)} | \hat{\mathbf{z}}, \mathbf{z}^{(1)}, \dots, \mathbf{z}^{(m-1)}) \\ &\stackrel{(b)}{\geq} H(\mathbf{z}^{(m)}) - H(\mathbf{z}^{(m)} | \hat{\mathbf{z}}) \\ &\stackrel{(c)}{\geq} H(\mathbf{z}^{(m)}) - H(\mathbf{z}^{(m)} | \hat{\mathbf{z}}^{(m)}) \\ &= I(\mathbf{z}^{(m)}; \hat{\mathbf{z}}^{(m)}), \end{aligned} \quad (45)$$

where (a) follows from (44), and (b) and (c) follows from the fact that conditioning always reduce the entropy. Substituting (45) into (44) proves (42). \square

Lemma 2. *Suppose that $\mathbf{z} \in \mathbb{C}^d$ is a complex Gaussian random vector with i.i.d. components $z_k \sim \mathcal{CN}(0, P)$. Let \mathbf{y} be any other random vector with correlation coefficient,*

$$\rho := \frac{|\mathbb{E}(\mathbf{z}^H \mathbf{y})|^2}{\mathbb{E}\|\mathbf{y}\|^2 \mathbb{E}\|\mathbf{z}\|^2} = \frac{|\mathbb{E}(\mathbf{z}^H \mathbf{y})|^2}{\mathbb{E}\|\mathbf{y}\|^2 P d}.$$

Then, the mutual information between \mathbf{z} and \mathbf{y} is bounded below by,

$$I(\mathbf{z}; \mathbf{y}) \geq -d \ln(1 - \rho).$$

Proof. The mutual information is,

$$I(\mathbf{z}; \mathbf{y}) = H(\mathbf{z}) - H(\mathbf{z} | \mathbf{y}). \quad (46)$$

Since \mathbf{z} is i.i.d. with d components distributed as $\mathcal{CN}(0, P)$,

$$H(\mathbf{z}) = d \ln(\pi e P). \quad (47)$$

Now, given \mathbf{y} , \mathbf{z} will have a conditional variance,

$$\sigma^2 := \frac{1}{d} \mathbb{E} [\|\mathbf{z} - \hat{\mathbf{z}}(\mathbf{y})\|^2], \quad (48)$$

where $\hat{\mathbf{z}}(\mathbf{y})$ is the MMSE estimator of \mathbf{z} given \mathbf{y} . So, the conditional entropy $H(\mathbf{z} | \mathbf{y})$ is bounded below by the entropy of the Gaussian,

$$H(\mathbf{z} | \mathbf{y}) \leq d \ln(\pi e \sigma^2). \quad (49)$$

But, we can further bound $H(\mathbf{z} | \mathbf{y})$ by replacing σ^2 with the variance for a linear estimator,

$$\sigma^2 \leq \frac{1}{d} \left[\mathbb{E}\|\mathbf{z}\|^2 - \frac{\mathbb{E}\|\mathbf{z}^H \mathbf{y}\|^2}{\mathbb{E}\|\mathbf{y}\|^2} \right] = \frac{1}{d} \left[P - \frac{|\mathbb{E}(\mathbf{z}^H \mathbf{y})|^2}{\mathbb{E}\|\mathbf{y}\|^2} \right]. \quad (50)$$

Therefore, substituting (47), (49) and (50) into (46),

$$I(\mathbf{z}; \mathbf{y}) \geq d \ln(\pi e P) - d \ln(\pi e \sigma^2) \geq -d \ln(1 - \rho). \quad \square$$

We use these lemmas as follows. In each sub-band m , the components of $\mathbf{z}^{(m)}$ are i.i.d. complex Gaussians with zero mean and variance P_m . So, by Lemma 2,

$$I(\mathbf{z}^{(m)}; \hat{\mathbf{z}}^{(m)}) \geq -N_m \ln(1 - \rho^{(m)}), \quad (51)$$

where N_m is the number of coefficients in sub-band m and $\rho^{(m)}$ is the correlation coefficient,

$$\rho^{(m)} := \frac{|\mathbb{E}((\mathbf{z}^{(m)})^H \hat{\mathbf{z}}^{(m)})|^2}{\mathbb{E}\|\hat{\mathbf{z}}^{(m)}\|^2 P_m}. \quad (52)$$

Now, (6) shows that $N_m/N \rightarrow \delta_m$. So, if we divide (51) by N and take the limit we get,

$$\liminf_{N \rightarrow \infty} \frac{1}{N} I(\mathbf{z}^{(m)}; \hat{\mathbf{z}}^{(m)}) \geq -\delta_m \ln(1 - \bar{\rho}^{(m)}). \quad (53)$$

where $\bar{\rho}^{(m)}$ is the limiting correlation,

$$\bar{\rho}^{(m)} := \lim_{N \rightarrow \infty} \rho^{(m)} \quad (54)$$

To compute the limiting correlation in (58), we use a similar calculation to the proof of Theorem 1. Specifically, the received symbols are given by,

$$\hat{\mathbf{z}} = \mathbf{V}\mathbf{G}(\mathbf{V}^H \mathbf{z} + \boldsymbol{\xi}).$$

Proposition 1 then shows that the components of $(\hat{\mathbf{z}}, \mathbf{z}, \mathbf{a})$ converge empirically as,

$$\lim_{N \rightarrow \infty} \{(\hat{z}_n, z_n, a_n)\} \stackrel{PL(2)}{=} (\hat{Z}, Z, A),$$

and

$$\hat{Z} = \alpha_{\text{rx}} Z + W_{\text{rx}}, \quad W_{\text{rx}} \sim \mathcal{CN}(0, \tau_{\text{rx}} \bar{P}),$$

where W_{rx} is independent of Z . Now, we have that,

$$\begin{aligned} \lim_{N \rightarrow \infty} \frac{1}{N} (\mathbf{z}^{(m)})^H \hat{\mathbf{z}}^{(m)} &= \lim_{N \rightarrow \infty} \frac{1}{N} z_k^* \hat{z}_k \mathbb{1}_{\{a_k=m\}} \\ &= \mathbb{E} [Z^* \hat{Z} \mathbb{1}_{\{A=m\}}] = \mathbb{E} [\bar{Z} \hat{Z} | A=m] \Pr(A=m) \\ &= \mathbb{E} [Z^* (\alpha_{\text{rx}} Z + W_{\text{rx}}) | A=m] \delta_m \\ &= \alpha_{\text{rx}} P_m \delta_m, \end{aligned}$$

where we have used that, conditional on $A=m$, $\mathbb{E}|Z|^2 = P_m$ and $\mathbb{E}(Z^* W_{\text{rx}}) = 0$. Hence,

$$\lim_{N \rightarrow \infty} \frac{1}{N^2} \left| \mathbb{E}(\mathbf{z}^{(m)})^H \hat{\mathbf{z}}^{(m)} \right|^2 = |\alpha_{\text{rx}}|^2 P_m^2 \delta_m^2. \quad (55)$$

Similar calculations show that,

$$\lim_{N \rightarrow \infty} \frac{1}{N} \mathbb{E}\|\hat{\mathbf{z}}^{(m)}\|^2 = [|\alpha_{\text{rx}}|^2 P_m + \tau_{\text{rx}} \bar{P}] \delta_m \quad (56)$$

$$\lim_{N \rightarrow \infty} \frac{1}{N} \mathbb{E}\|\mathbf{z}^{(m)}\|^2 = P_m \delta_m. \quad (57)$$

Substituting (55), (56) and (57) into (52), we obtain that the limit in (58) is given by,

$$\bar{\rho}^{(m)} := \frac{|\alpha_{\text{rx}}|^2 P_m^2 \delta_m^2}{P_m [|\alpha_{\text{rx}}|^2 P_m + \tau_{\text{rx}} \bar{P}] \delta_m^2} = \frac{|\alpha_{\text{rx}}|^2 P_m}{|\alpha_{\text{rx}}|^2 P_m + \tau_{\text{rx}} \bar{P}}. \quad (58)$$

Hence, from (53), we obtain

$$\liminf_{N \rightarrow \infty} \frac{1}{N} I(\mathbf{z}^{(m)}; \hat{\mathbf{z}}^{(m)}) \geq \delta_m \log \left(1 + \frac{|\alpha_{\text{rx}}|^2 P_m}{\tau_{\text{rx}} \bar{P}} \right). \quad (59)$$

Substituting (59) into the sum (42) obtains (17).

APPENDIX F PROOF OF THEOREM 3

This is a straightforward mathematical manipulation

$$\begin{aligned} R_{\text{lin}} &\stackrel{(a)}{\geq} \sum_{m=1}^M \delta_m \log \left(1 + \frac{|\alpha_{\text{tx}}|^2 P_m}{\tau_{\text{tx}} \bar{P}} \right) \\ &= \sum_{m=1}^M \delta_m \log \left(\frac{\tau_{\text{tx}} \bar{P} + |\alpha_{\text{tx}}|^2 P_m}{\tau_{\text{tx}} \bar{P}} \right) \\ &\stackrel{(b)}{=} \sum_{m=1}^M \delta_m \log \left(\frac{\nu_m (|\alpha_{\text{tx}}|^2 + \tau_{\text{tx}} \bar{P})}{\delta_m \tau_{\text{tx}} \bar{P}} \right) \\ &= \log \left(1 + \frac{|\alpha_{\text{tx}}|^2}{\tau_{\text{tx}}} \right) + \sum_{m=1}^M \delta_m \log \left(\frac{\nu_m}{\delta_m} \right) \\ &= \log \left(1 + \frac{|\alpha_{\text{tx}}|^2}{\tau_{\text{tx}}} \right) - D(\boldsymbol{\delta} \| \boldsymbol{\nu}). \end{aligned}$$

where (a) follows from (20) with $\sigma^2 = 0$ and (b) follows from (12). This proves (21).

APPENDIX G PROOF OF THEOREM 4

We first need a lemma to characterize the maximum entropy, $H_{\text{max}}(s)$ in (28). Let S be a random variable given by $|x|^2$ where x uniformly distributed on the set of DAC constellation points $x \in A$. Hence, $\mathbb{E}(S)$ is the average energy per sample if the modulator uniformly selects sequences from the DAC output. Let $\lambda_S(\theta)$ be its cumulant generating function,

$$\lambda_S(\theta) = \log \mathbb{E} \exp(\theta S) = \log \left(\frac{1}{|A|} \sum_{x \in A} e^{\theta |x|^2} \right), \quad (60)$$

and, let $I_S(s)$ be its Legendre transform,

$$I_S(s) := \sup_{\theta} [\theta s - \lambda(\theta)]. \quad (61)$$

Lemma 3. The maximum entropy in (28) is given by,

$$H_{\text{max}}(s) = \log |A| - I_S(s). \quad (62)$$

Proof. Consider a set of distributions of a discrete random variable V_{θ} on the set A , parameterized by the scalar real variable θ , where

$$P(V_{\theta} = x) = \frac{1}{|A| Z(\theta)} e^{\theta |x|^2}, \quad Z(\theta) = \frac{1}{|A|} \sum_{x \in A} e^{\theta |x|^2}. \quad (63)$$

It is known that if θ is selected such that $\mathbb{E}|V_{\theta}|^2 = s$, then V_{θ} is the maximum entropy distribution over all random variables V

on A with $\mathbb{E}|V|^2 = s$. Observe that the cumulant generating function (60) is,

$$\lambda_S(\theta) = \log Z(\theta).$$

A standard result on exponential families is that,

$$\lambda'_S(\theta) = \mathbb{E}|V_\theta|^2.$$

Now, for any s , we have

$$I_S(s) = \hat{\theta}s - \lambda_S(\hat{\theta}),$$

where

$$\hat{\theta} = \arg \max_{\theta} [s\theta - \lambda_S(\theta)]. \quad (64)$$

Since $\hat{\theta}$ is the maximizer in (64),

$$\lambda'_S(\hat{\theta}) = s \Rightarrow s = \mathbb{E}|V_{\hat{\theta}}|^2.$$

So, $V_{\hat{\theta}}$ is the maximum entropy distribution with $E|V|^2 = s$. Also, the entropy of PMF of $V_{\hat{\theta}}$ in (63) is,

$$\begin{aligned} H_{\max}(s) &= H(V_{\hat{\theta}}) = -\mathbb{E} \log P(V_{\hat{\theta}}) \\ &= \log |A| + \log Z(\hat{\theta}) - \hat{\theta} \mathbb{E}|V_{\hat{\theta}}|^2 \\ &= \log |A| + \log \lambda_S(\hat{\theta}) - \hat{\theta}s \\ &= \log |A| - I_S(s). \end{aligned} \quad (65)$$

□

We now proceed to the proof of Theorem 4. There are $|A|^N$ sequences in the set A^N . So, if we let \mathbf{x}_N be the random vector uniformly generated on A^N , we have that the expected cardinality of the set $G_N(\mathbf{V}, \epsilon)$ in (23) is,

$$\mathbb{E}|G_N(\mathbf{V}, \epsilon)| = |A|^N \Pr(\phi(\mathbf{V}\mathbf{x}_N) \in [s - \epsilon, s]),$$

where the probability is taken over the random vector \mathbf{x}_N and the matrix \mathbf{V} . Hence, the rate upper bound in (25) is

$$\bar{R} = \ln |A| + \lim_{\epsilon \rightarrow 0} \lim_{N \rightarrow \infty} \frac{1}{N} \ln \Pr(\phi(\mathbf{V}\mathbf{x}_N) \in [s - \epsilon, s]). \quad (66)$$

So, we need to compute a tail probability. This is a standard large deviations calculation. Define the random variable,

$$S_N := \frac{1}{N} \|\mathbf{x}_N\|^2, \quad (67)$$

which represents the per sample total energy in the vector \mathbf{x}_N . Also, let \mathbf{u}_N be the unit vector,

$$\mathbf{u}_N = \frac{1}{\|\mathbf{x}_N\|} \mathbf{V}\mathbf{x}_N = \frac{1}{\|\mathbf{V}\mathbf{x}_N\|} \mathbf{V}\mathbf{x}_N. \quad (68)$$

Since \mathbf{V} is Haar distributed on the unitaries, \mathbf{u}_N is uniformly distributed on the sphere of radius one and independent of \mathbf{x}_N . Also, let

$$\nu_{N,m} := \frac{1}{N} \sum_{k=0}^{N-1} \mathbb{1}_{\{a_k=m\}} |u_k|^2, \quad (69)$$

which is the fraction of the energy of \mathbf{u} in sub-band m . With these definitions, if $\mathbf{r} = \mathbf{V}\mathbf{x}$ the sub-band energies in (3) is given by,

$$\begin{aligned} \phi_m(\mathbf{r}) &:= \frac{1}{N} \sum_{k=0}^{N-1} |r_k|^2 \mathbb{1}_{\{a_k=m\}} \\ &\stackrel{(a)}{=} \frac{1}{N} \|\mathbf{x}\|^2 \sum_{k=0}^{N-1} |u_k|^2 \mathbb{1}_{\{a_k=m\}} \stackrel{(b)}{=} S_N \nu_{N,m} \end{aligned} \quad (70)$$

where (a) holds since $\mathbf{r} = \mathbf{V}\mathbf{x} = \|\mathbf{x}\|^2 \mathbf{u}$, and (b) holds from the definition of S_N in $\nu_{N,m}$ in (67) and (69). So, $\mathbf{x}_N \in G_N(\mathbf{V}, \epsilon)$ if and only if,

$$S_N \nu_{N,m} \in [s_m - \epsilon, s_m] \quad (71)$$

for all m . Therefore, if we define the set,

$$G_\epsilon := \{(s, \boldsymbol{\nu}) \mid s\nu_m \in [s_m - \epsilon, s_m]\}, \quad (72)$$

the constraint (71) can be written as $(S_N, \boldsymbol{\nu}_N) \in G_\epsilon$, and the rate upper bound (66) is given by,

$$\bar{R} = \ln |A| + \lim_{\epsilon \rightarrow 0} \lim_{N \rightarrow \infty} \frac{1}{N} \ln \Pr((S_N, \boldsymbol{\nu}_N) \in G_\epsilon). \quad (73)$$

We will calculate the probability using large deviations.

First, since S_N in (67) is given by,

$$S_N = \frac{1}{N} \sum_{n=0}^{N-1} |x_n|^2,$$

which is an empirical average of i.i.d. random variables with distribution S , the random variable $|x|^2$ where x is uniformly distributed on the DAC constellation points A . By Cramer's theorem, it satisfies the large deviations principle (LDP) with rate function, $I_S(s)$ [43].

Also, each component $\nu_{N,m}$ is the energy fraction of the projection of an N -dimensional complex unit vector onto a sub-space of dimension N_m with $N_m = \delta_m N$. Thus, $\boldsymbol{\nu}_N$ has the Dirchelet distribution with probability density,

$$p(\boldsymbol{\nu}_N) = \frac{1}{B(\boldsymbol{\alpha})} \prod_{m=1}^M \nu_{N,m}^{\alpha_m - 1},$$

where $\boldsymbol{\alpha}$ is the vector with coefficients,

$$\alpha_m = N\delta_m,$$

and

$$B(\boldsymbol{\alpha}) = \frac{\prod_m \Gamma(\alpha_m)}{\Gamma(\sum_m \alpha_m)}.$$

Using Sterling's approximation for large N , the density is approximately given by,

$$p(\boldsymbol{\nu}_N) \approx \exp[-ND(\boldsymbol{\delta} \|\boldsymbol{\nu})].$$

Therefore, $\boldsymbol{\nu}_N$ satisfies the LDP with rate function

$$I_{\boldsymbol{\nu}}(\boldsymbol{\nu}) = D(\boldsymbol{\delta} \|\boldsymbol{\nu}).$$

Since S_N and $\boldsymbol{\nu}_N$ are independent, they have a rate $I_S(s) + I_{\boldsymbol{\nu}}(\boldsymbol{\nu})$. By the property of the rate function,

$$\begin{aligned} \lim_{N \rightarrow \infty} \frac{1}{N} \ln \Pr((S_N, \boldsymbol{\nu}_N) \in G_\epsilon) \\ = - \inf_{s, \boldsymbol{\nu} \in G_\epsilon} [I_S(s) + D(\boldsymbol{\delta} \|\boldsymbol{\nu})]. \end{aligned} \quad (74)$$

Using the definition of (72) and the fact that $I_S(s)$ is continuous, we obtain

$$\begin{aligned} \lim_{\epsilon \rightarrow 0} \lim_{N \rightarrow \infty} \frac{1}{N} \ln \Pr((S_N, \boldsymbol{\nu}_N) \in G_\epsilon) \\ = - \inf_{s, \boldsymbol{\nu} \in G_0} [I_S(s) + D(\boldsymbol{\delta} \parallel \boldsymbol{\nu})]. \end{aligned} \quad (75)$$

But, taking $\epsilon = 0$ in (72), we see that G_0 is the set

$$G_\epsilon := \{(S, \boldsymbol{\nu}) \mid s\nu_m = s_m \ \forall m\}.$$

Since $\sum_m \nu_m = 1$, the only point in G_0 are the $s = s_{\text{tot}} =$

$\sum_m s_m$ and $\nu_m = s_m/s_{\text{tot}}$. Therefore,

$$\begin{aligned} \lim_{\epsilon \rightarrow 0} \lim_{N \rightarrow \infty} \frac{1}{N} \ln \Pr((S_N, \boldsymbol{\nu}_N) \in G_\epsilon) \\ = -I_S(s_{\text{tot}}) - D(\boldsymbol{\delta} \parallel \boldsymbol{\nu}). \end{aligned}$$

Substituting this into (73),

$$\bar{R} = \ln |A| - I_S(s_{\text{tot}}) - D(\boldsymbol{\delta} \parallel \boldsymbol{\nu}). \quad (76)$$

From Lemma 3, this can be re-written as,

$$\bar{R} = H_{\text{max}}(s_{\text{tot}}) - D(\boldsymbol{\delta} \parallel \boldsymbol{\nu}). \quad (77)$$